Tunnel electroresistance in BiFeO3 junctions: size does matter

Tunnel electroresistance in $BiFeO_3$ junctions: size does matter

S. Boyn[1], A.M. Douglas[2], C. Blouzon[3], P. Turner[2], A. Barthélémy[1], M. Bibes[1], S. Fusil[1], J.M. Gregg[2], V. Garcia[11]

[1] *Unité Mixte de Physique, CNRS, Thales, Univ. Paris-Sud, Université Paris-Saclay, 91767, Palaiseau, France*

[2] *Centre for Nanostructured Media, School of Mathematics and Physics, Queen's University Belfast, University Road, Belfast BT7 1NN, United Kingdom*

[3] *Service de Physique de l'Etat Condensé, CEA Saclay, DSM/IRAMIS/SPEC, URA CNRS 2464, 91191 Gif-sur-Yvette, France*

In ferroelectric tunnel junctions, the tunnel resistance depends on the polarization orientation of the ferroelectric tunnel barrier, giving rise to tunnel electroresistance. These devices are promising to be used as memristors in neuromorphic architectures and as non-volatile memory elements. For both applications device scalability is essential, which requires a clear understanding of the relationship between polarization reversal and resistance change as junction size shrinks. Here we show robust tunnel electroresistance in $BiFeO_3$-based junctions with diameters ranging from 1200 to 180 nm. We demonstrate that the tunnel electroresistance and the corresponding fraction of reversed ferroelectric domains change

[1] Electronic mail: vincent.garcia@thalesgroup.com

drastically with the junction diameter: while micron-size junctions display reversal in less than 10% of the area, the smallest junctions show an almost complete polarization reversal. Modeling the electric-field distribution, we highlight the critical role of the bottom electrode resistance which significantly diminishes the actual electric field applied to the ferroelectric barrier in the mixed polarization state. A polarization-dependent critical electric field below which further reversal is prohibited is found to explain the large differences between the ferroelectric switchability of nano- and micron-size junctions. Our results indicate that ferroelectric junctions are downscalable and suggest that specific junction shapes facilitate complete polarization reversal.

Ferroelectric materials possess a spontaneous electrical polarization that is switchable by an external electric field. This enables the use of thin ferroelectric films sandwiched between electrodes as non-volatile memories.[1] In such ferroelectric memories, the information is encoded by the polarization orientation and recovered in a destructive capacitive readout. When the thickness of the ferroelectric films is of the order of a few nanometers, electron tunneling becomes possible. In these ferroelectric tunnel junctions,[2,3] the tunnel resistance varies depending on the orientation of the polarization; this tunnel electroresistance effect enables a non-destructive information readout.[4–6] Furthermore, ferroelectric domains and their dynamics[7–10] offer additional degrees of freedom and give rise to an analog memristive response of the tunnel junction[11–14] that emulates the behavior of synapses in neuromorphic networks.[15,16]

Large tunnel electroresistance values of more than 10^3 are now achievable at room temperature,[17–21] which makes ferroelectric tunnel junctions interesting candidates for resistive memories.[3] In addition, coupling ferroelectric materials to strongly correlated oxide electrodes can provide a local, permanent, and switchable electric field able to trigger electronic or magnetic phase transitions.[22] In tunnel junctions combined with ferromagnetic electrodes for example, the polarization reversal can induce changes of the interfacial magnetization.[23–25] These interfacial magnetoelectric coupling phenomena can be probed by tunnel magnetoresistance experiments, resulting in a non-volatile control of the spin-polarization.[26–29] Moreover, selecting oxide electrodes subject to field-induced electronic phase transitions upon polarization reversal may result in enhanced tunnel electroresistance.[29,30] Hence, ferroelectric tunnel junctions offer a fantastic playground to explore electric-field-driven modifications at the nanoscale.[3]

However, pure tunnel electroresistance measurements do not provide any information on the efficiency of polarization switching: since the first nanodomain with high conductivity nucleating from a homogeneously polarized state (OFF resistance) acts as a "shortcut", it immediately leads to large electrical contrasts.[11,18] For such an incomplete polarization reversal, the effect of field-induced modifications of electronic or magnetic properties would be confined to a minor fraction of the junction area. Therefore, a thorough understanding of interfacial field-effect modifications requires a precise knowledge of the polarization landscape in ferroelectric tunnel junctions. In this paper, we demonstrate that the efficiency of polarization switching and the corresponding tunnel electroresistance strongly vary with the lateral size of $BiFeO_3$-based tunnel junctions. The experimental size-dependent polarization configurations are understood

by electric-field distribution simulations that reveal the significant role of the oxide electrode resistance. These results underline the peculiar interplay between geometry and domain populations in such conductive ferroelectric films.

Ferroelectric tunnel junctions are fabricated from epitaxial heterostructures of $BiFeO_3$ (4.6 nm) / $Ca_{0.96}Ce_{0.04}MnO_3$ (21 nm) grown by pulsed laser deposition on $YAlO_3$ substrates.[18] The large epitaxial strain imposed by the substrate stabilizes $BiFeO_3$ in its super-tetragonal polymorphic phase with a large polarization that initially points towards the $Ca_{0.96}Ce_{0.04}MnO_3$ bottom electrode.[31] Top electrodes of Pt (10 nm) / Co (10 nm) with diameters ranging from 180 nm to 1200 nm (Fig. 1(a)) are defined by electron-beam lithography, sputtering, and lift-off.[18] We use the conductive tip of an atomic force microscope (AFM) to connect individual top electrodes and perform electric transport measurements under a constant voltage of −100 mV after applying voltage pulses of 100 ns with amplitudes ranging from −3.5 V to 3.5 V. The bottom electrode is connected to ground. We use this AFM set-up to map ferroelectric domains by piezoresponse force microscopy (PFM) through the top electrode.

Fig. 1(b) shows resistance hysteresis cycles as a function of the amplitude of write voltage pulses for five different junction diameters. All junctions show large tunnel electroresistance with two well-defined ON and OFF resistance states and are initially in the OFF state. The reversibility of the switching between these two states is emphasized by the virtually undistinguishable first and second cycles (open and full symbols, respectively) for all junctions. Strikingly, the tunnel electroresistance decreases as the junction diameter increases. It reaches about 5×10^4 for 180-nm-wide junctions and only 6×10^2 for the 1200-nm ones.

In general, one would not expect the tunnel electroresistance to depend on the lateral size of the junctions. Indeed, the resistance-area product of a junction in a homogeneous state of polarization should be constant if tunnel transport is involved. Figure 2 displays the ON and OFF resistance-area products as a function of the device diameter and the corresponding ferroelectric domain populations. The resistance-area product of the OFF resistance state does not vary with the junction diameter. This indicates a good structural and electrical homogeneity of the $BiFeO_3$ tunnel barrier under the assumption of a homogeneous polarization state up to the micron scale. This is corroborated by the bright PFM phase and constant PFM amplitude for all OFF resistance states (Fig. 2(b)) which indicate a homogeneous polarization pointing downward (toward the $Ca_{0.96}Ce_{0.04}MnO_3$ electrode) for all device sizes.

In the ON resistance state however, the resistance-area product increases as the junction diameter increases (Fig. 2(a)). This suggests that the switching behavior may change with the junction size. Indeed, the PFM phase images of junctions in the ON resistance state are strikingly different (Fig. 2(b)): for 180-nm junctions, the ON-state PFM phase is almost completely dark, suggesting that a majority of the ferroelectric domains have switched from downward to upward (toward the Co electrode); for 290-nm junctions, the mixed PFM phase signal indicates that only half of the area is switched, while for the 1200-nm junctions, a majority of domains remain in the downward state. In Figure 2(c), the ON-state fraction of reversed domains (upward polarization) is estimated from the PFM phase images (Fig. 2(b)) and plotted as a function of the junction diameter. We conclude that the decrease of the tunnel electroresistance with the junction diameter can be explained by a reduced fraction of switched ferroelectric domains in the ON resistance state.

In order to get more insights into the size-dependent polarization reversal of these $BiFeO_3$ tunnel junctions, we perform finite-size-element electric-field distribution simulations (using the Quickfield software, Fig. 3). In these 2D simulations, a voltage of −3.5 V is applied to the top electrode of Co while each end of a 10-µm-long bottom electrode of $Ca_{0.96}Ce_{0.04}MnO_3$ is connected to ground (Fig. 3(a)). We consider the resistivity of the $Ca_{0.96}Ce_{0.04}MnO_3$ electrode (5 mΩ.cm) as measured experimentally in patterned junctions [32]. In addition, the actual values of the resistance area products for the up (9×10^2 Ω.µm²) and down (2×10^4 Ω.µm²) domains in this voltage range are deduced from real-time transmission experiments and dc measurements (not shown). Owing to the pronounced non-linearity of tunnel transport, these resistance-area products during voltage pulses of −3.5 V are significantly lower than in the low dc voltage range we use for hysteresis (Fig. 1(b)).

In the initial state of 180-nm-wide junctions (OFF resistance, downward polarization, Fig. 3(a)), the voltage mainly drops across the $BiFeO_3$ tunnel barrier (Fig. 3(b)), giving rise to a homogeneous electric field in the center of the junction (Fig. 3(c)). This electric field strongly increases at the edge of the top electrode (Fig. 3(c)), which should favor the nucleation of ferroelectric domains with up polarization in agreement with experimental PFM observations (Fig. 2(b)). The introduction of domains with up polarization at the edges of the junction (Fig. 3(d)), during the OFF-to-ON switching, induces a change of the voltage profile (Fig. 3(e)) and a strong reduction of the electric field within the unswitched central region of the $BiFeO_3$ tunnel barrier (Fig. 3(f)). This can be understood by considering the fact that as up domains switch, the equivalent resistance of the tunnel barrier comes close to that of the

$Ca_{0.96}Ce_{0.04}MnO_3$ electrode. Consequently, a significant part of the voltage drops within the electrode, as emphasized in Fig. 3(g).

The electric-field simulations are repeated for various fractions of domains with up polarization and for 180-nm- and 1200-nm-wide top electrodes. The resulting evolution of the electric field in the unswitched center of the barrier as a function of the domain proportion is plotted in Figure 4. In the case of a homogeneous polarization pointing downward (corresponding to the OFF-resistance state in the experiments), the electric field in $BiFeO_3$ is smaller for 1200-nm-wide junctions than for 180-nm ones. As the fraction of up domains increases this difference becomes larger. Considering a critical field below which no down domains can be switched (horizontal line in Fig. 4(a)), these simple simulations can qualitatively explain the experiments with $BiFeO_3$ tunnel junctions. For a critical field of 0.48 V/nm, about 80% of up domains can be formed in 180-nm-wide junctions while less than 10% will reverse in 1200-nm-wide junctions. These estimates fall within the range of our experimental observations by PFM (Fig. 2(b)-(c)) for the ON resistance states of junctions with various sizes.

The electric-field simulations thus demonstrate the influence of the electrode resistance on the efficiency of polarization switching in ferroelectric tunnel junctions; this series resistance may impede the full reversal of polarization, limiting the tunnel electroresistance. We note that a total polarization reversal is not achieved for the junctions reported here, even for the smallest devices. In view of the promising applications mentioned above, ways to circumvent this issue are highly desirable. We recall that the nucleation takes place at the edges of the junction, where the electric field is stronger. The field across the barrier continuously decreases as the upward domains grow, until it reaches a critical value at which the domains freeze, the switched

area being defined by the specific switching dynamics of the tunnel junctions. Indeed, here, the electric field is highly dependent on the domain configuration, which is not the case for classical (thick insulating film) ferroelectric capacitors used in ferroelectric memories.[1]

Exploiting the increased electric field at the edges (Fig. 3(c)) in junctions with large areas but high perimeter-to-area ratios could be an efficient trick to improve the switching efficiency. This is illustrated in Fig. 5 where the polarization reversals of two junctions with similar areas but different perimeter-to-area ratios are compared. In the donut-shaped junction (Fig. 5(a)), the increased electric field at the inner and outer edges promotes domain nucleation (as visible from the PFM amplitude in the intermediate state). This enables a more efficient switching of polarization than in the circular junction with similar area (Fig. 5(b)). Consequently, the fraction of up domains (dark PFM phase in the images) is higher for the donut than for the disk in the ON state. The resulting tunnel electroresistance reaches 2.5×10^4 for the donut, which is about three times higher than in the circular junction with a similar area.

We report a peculiar size dependence of the tunnel electroresistance linked to an incomplete polarization switching in ferroelectric tunnel junctions based on $BiFeO_3$. Larger tunnel electroresistances are obtained for smaller junctions. Electric field simulations give some insights into the critical role of the oxide electrode resistance during polarization reversal, which limits the actual field applied to the ferroelectric in the mixed polarization state. Optimizing the geometry of the junctions provides a way to improve the switchability of the device. In contrast to thick insulating ferroelectric capacitors, the actual electric field across the ferroelectric tunnel barrier evolves dynamically with the domain population, resulting in potentially complex

dynamic behavior. Resorting to smartly designed nanoscale devices could yield efficient polarization switching and maximize the tunnel electroresistance.

ACKNOWLEDGEMENTS

We thank Hiroyuki Yamada, Cécile Carrétéro, Cyrile Deranlot, and Stéphane Xavier for technical assistance with the sample fabrication. Financial support from the French Agence Nationale de la Recherche (ANR) through project FERROMON and MIRA is acknowledged.

REFERENCES

[1] J.F. Scott, Science **315**, 954 (2007).

[2] E.Y. Tsymbal, Science **313**, 181 (2006).

[3] V. Garcia and M. Bibes, Nature Commun. **5**, 4289 (2014).

[4] V. Garcia, S. Fusil, K. Bouzehouane, S. Enouz-Vedrenne, N.D. Mathur, A. Barthélémy, and M. Bibes, Nature **460**, 81 (2009).

[5] P. Maksymovych, S. Jesse, P. Yu, R. Ramesh, A.P. Baddorf, and S. V Kalinin, Science **324**, 1421 (2009).

[6] A. Gruverman, D. Wu, H. Lu, Y. Wang, H.W. Jang, C.M. Folkman, M.Y. Zhuravlev, D. Felker, M. Rzchowski, C.-B. Eom, and E.Y. Tsymbal, Nano Lett. **9**, 3539 (2009).

[7] M. Dawber, K.M. Rabe, and J.F. Scott, Rev. Mod. Phys. **77**, 1083 (2005).

[8] A. Gruverman, D. Wu, and J. Scott, Phys. Rev. Lett. **100**, 097601 (2008).

[9] A. Gruverman, J. Mater. Sci. **44**, 5182 (2009).

[10] D. Lee, S.M. Yang, T.H. Kim, B.C. Jeon, Y.S. Kim, J.-G. Yoon, H.N. Lee, S.H. Baek, C.B. Eom, and T.W. Noh, Adv. Mater. **24**, 402 (2012).

[11] A. Chanthbouala, V. Garcia, R.O. Cherifi, K. Bouzehouane, S. Fusil, X. Moya, S. Xavier, H. Yamada, C. Deranlot, N.D. Mathur, M. Bibes, A. Barthélémy, and J. Grollier, Nature Mater. **11**, 860 (2012).

[12] D.J. Kim, H. Lu, S. Ryu, C.-W. Bark, C.-B.B. Eom, E.Y. Tsymbal, and A. Gruverman, Nano Lett. **12**, 5697 (2012).

[13] A. Quindeau, D. Hesse, and M. Alexe, Front. Phys. **2**, 1 (2014).

[14] Z. Wen, D. Wu, and A. Li, Appl. Phys. Lett. **105**, 0 (2014).

[15] C. Zamarreño-Ramos, L.A. Camuñas-Mesa, J.A. Perez-Carrasco, T. Masquelier, T. Serrano-Gotarredona, and B. Linares-Barranco, Front. Neurosci. **5**, 26 (2011).

[16] L.F. Abbott and S.B. Nelson, Nature Neurosci. **3**, 1178 (2000).

[17] Z. Wen, C. Li, D. Wu, A. Li, and N. Ming, Nature Mater. **12**, 617 (2013).

[18] H. Yamada, V. Garcia, S. Fusil, S. Boyn, M. Marinova, A. Gloter, S. Xavier, J. Grollier, E. Jacquet, C. Carrétéro, C. Deranlot, M. Bibes, and A. Barthélémy, ACS Nano **7**, 5385 (2013).

[19] H. Lu, A. Lipatov, S. Ryu, D.J. Kim, H. Lee, M.Y. Zhuravlev, C.B. Eom, E.Y. Tsymbal, A. Sinitskii, and A. Gruverman, Nature Commun. **5**, 5518 (2014).

[20] L. Wang, M.R. Cho, Y.J. Shin, J.R. Kim, S. Das, J.-G. Yoon, J.-S. Chung, and T.W. Noh, Nano Lett. **16**, 3911 (2016).

[21] F.Y. Bruno, S. Boyn, S. Fusil, S. Girod, C. Carrétéro, M. Marinova, A. Gloter, S. Xavier, C. Deranlot, M. Bibes, A. Barthélémy, and V. Garcia, Adv. Electron. Mater. **2**, 1500245 (2016).

[22] C.H. Ahn, J.-M. Triscone, and J. Mannhart, Nature **424**, 1015 (2003).

[23] C. Duan, S. Jaswal, and E. Tsymbal, Phys. Rev. Lett. **97**, 047201 (2006).

[24] M.K. Niranjan, J.D. Burton, J.P. Velev, S.S. Jaswal, and E.Y. Tsymbal, Appl. Phys. Lett. **95**, 052501 (2009).

[25] J. Burton and E. Tsymbal, Phys. Rev. B **80**, 174406 (2009).

[26] V. Garcia, M. Bibes, L. Bocher, S. Valencia, F. Kronast, A. Crassous, X. Moya, S. Enouz-Vedrenne, A. Gloter, D. Imhoff, C. Deranlot, N.D. Mathur, S. Fusil, K. Bouzehouane, and A. Barthélémy, Science **327**, 1106 (2010).

[27] S. Valencia, A. Crassous, L. Bocher, V. Garcia, X. Moya, R.O. Cherifi, C. Deranlot, K. Bouzehouane, S. Fusil, A. Zobelli, A. Gloter, N.D. Mathur, A. Gaupp, R. Abrudan, F. Radu, A. Barthélémy, and M. Bibes, Nature Mater. **10**, 753 (2011).

[28] D. Pantel, S. Goetze, D. Hesse, and M. Alexe, Nature Mater. **11**, 289 (2012).

[29] Y.W. Yin, J.D. Burton, Y. Kim, A.Y. Borisevich, S.J. Pennycook, S.M. Yang, T.W. Noh, A. Gruverman, X.G. Li, E.Y. Tsymbal, and Q. Li, Nature Mater. **12**, 397 (2013).

[30] L. Jiang, W.S. Choi, H. Jeen, S. Dong, Y. Kim, M.-G. Han, Y. Zhu, S. V Kalinin, E. Dagotto, T. Egami, and H.N. Lee, Nano Lett. **13**, 5837 (2013).

[31] M. Marinova, J.E. Rault, A. Gloter, S. Nemsak, G.K. Palsson, J.-P. Rueff, C.S. Fadley, C. Carrétéro, H. Yamada, K. March, V. Garcia, S. Fusil, A. Barthélémy, O. Stéphan, C. Colliex, and M. Bibes, Nano Lett. **15**, 2533 (2015).

[32] S. Boyn, S. Girod, V. Garcia, S. Fusil, S. Xavier, C. Deranlot, H. Yamada, C. Carrétéro, E. Jacquet, M. Bibes, A. Barthélémy, and J. Grollier, Appl. Phys. Lett. **104**, 052909 (2014).

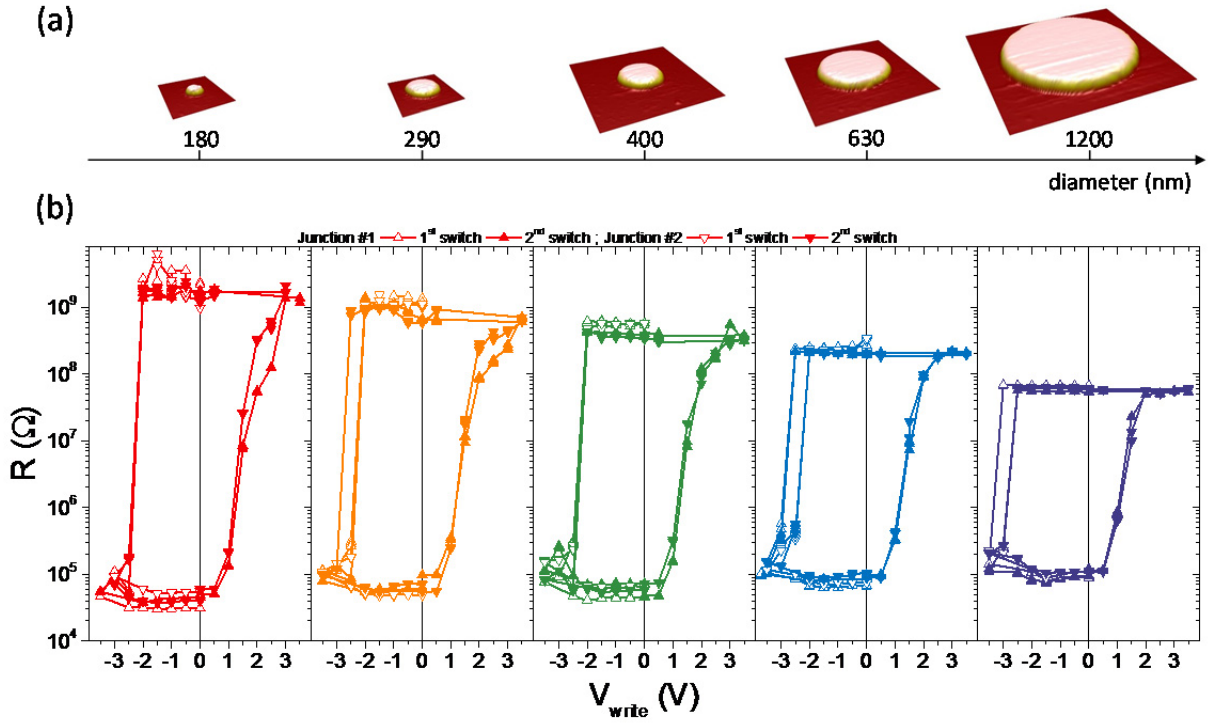

FIG. 1. (a) 3D topographic atomic force microscopy images of $BiFeO_3$ tunnel junction top electrodes with increasing diameters. (b) Resistance hysteresis with write voltage pulses for each junction diameter. The first two hysteresis cycles of two typical junctions are displayed for each diameter.

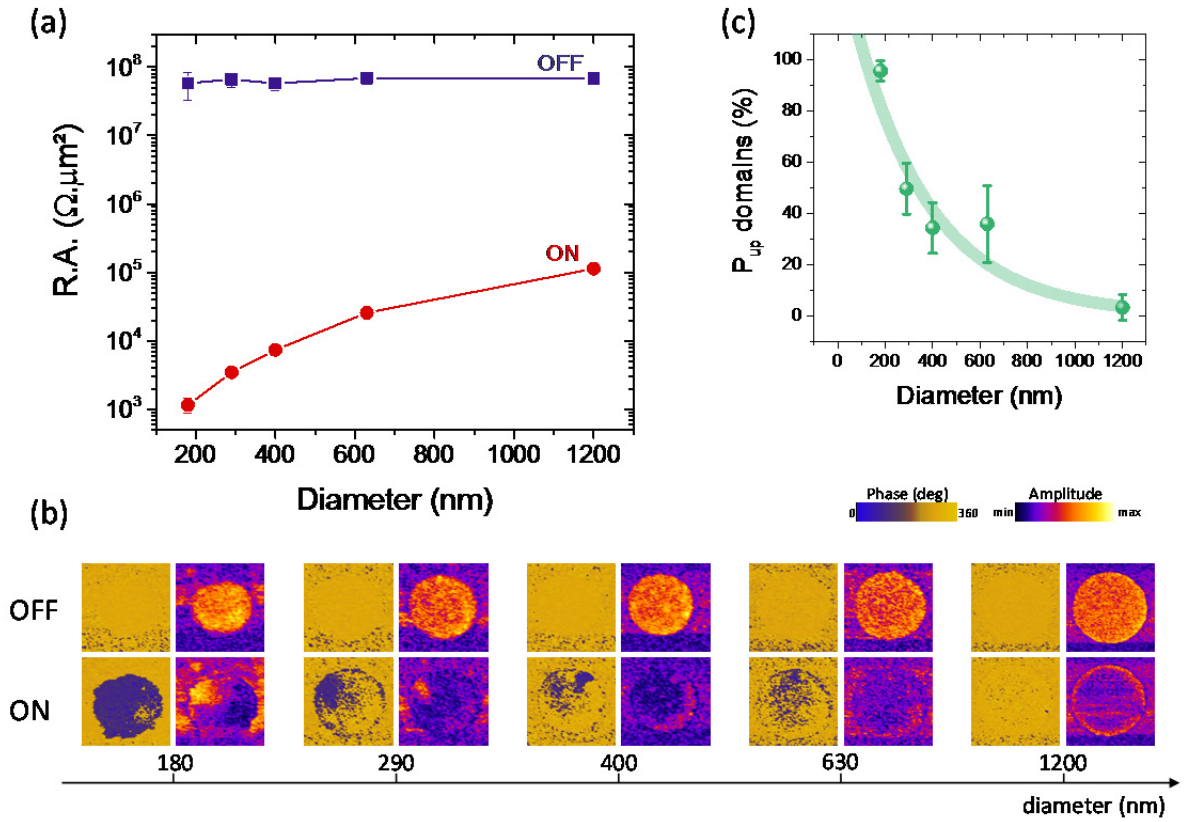

FIG. 2. (a) Resistance-area product in the OFF and ON states as a function of diameter of the tunnel junctions displayed in Figure 1b. (b) Piezoresponse force microscopy images (out-of-plane phase (left) and amplitude (right)) in the OFF and ON states of junctions with different diameters. (c) Fraction of domains with polarization pointing up in the ON state as a function of the junction diameter estimated from PFM phase images of (b). The line is a guide to the eyes.

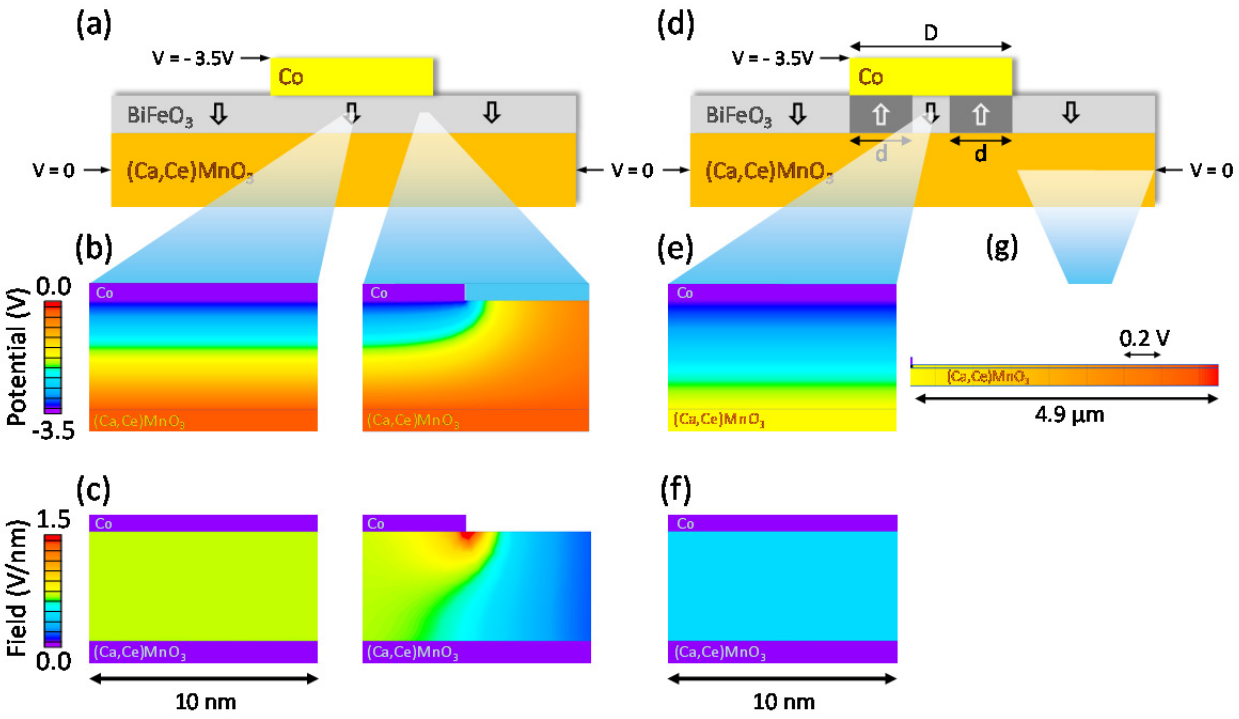

FIG. 3. (a) Schematic of the structure (not to scale) used for the model in the case of a uniform down polarization in $BiFeO_3$, considering a 180-nm-wide top electrode and 10-µm-long bottom electrode of $Ca_{0.96}Ce_{0.04}MnO_3$. The following parts (b-c) of the figure are zoomed in to 10 nm x 6.5 nm regions. (b) The potential drop and (c) uniform electric field found within the center of the junction can be compared with the edge of the top electrode region, whereby the potential distribution of the fringes creates an enhanced electric field, facilitating the nucleation of domains from this point. (d) Schematic of the same structure considering that up domains (with width d = 80 nm) switched from the edges of the junction. (e) The potential and (f) electric field distributions within the center of the junction show significant changes compared to the homogeneous state (b-c). Indeed, a significant part of the potential drops along the length of the bottom electrode of $Ca_{0.96}Ce_{0.04}MnO_3$ in the switched state as illustrated in (g).

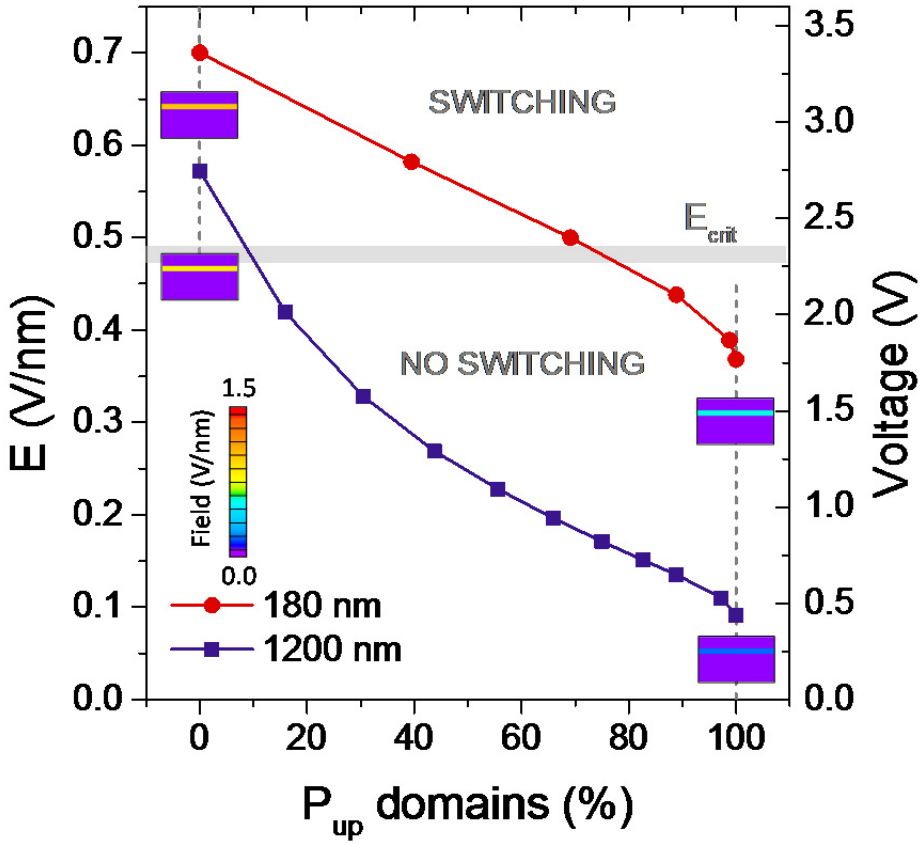

FIG. 4. Evolution of the electric field as up domains are introduced in the barrier, for 180-nm- and 1200-nm-wide junctions. The geometry used for the simulations is the same as in Figure 3d from which the fraction of upward domains is determined as $\frac{4d(D-d)}{D^2}$. The inset shows examples of the electric field distributions in 10 nm x 6.5 nm regions of the center of junctions for homogeneous up or down polarization states. The horizontal line is an estimate of the critical field below which up domains cannot nucleate. For the 100-ns pulses of −3.5 V studied here, this corresponds to a fraction of up domains of 12% and 86% for 1200-nm and 180-nm junctions, respectively.

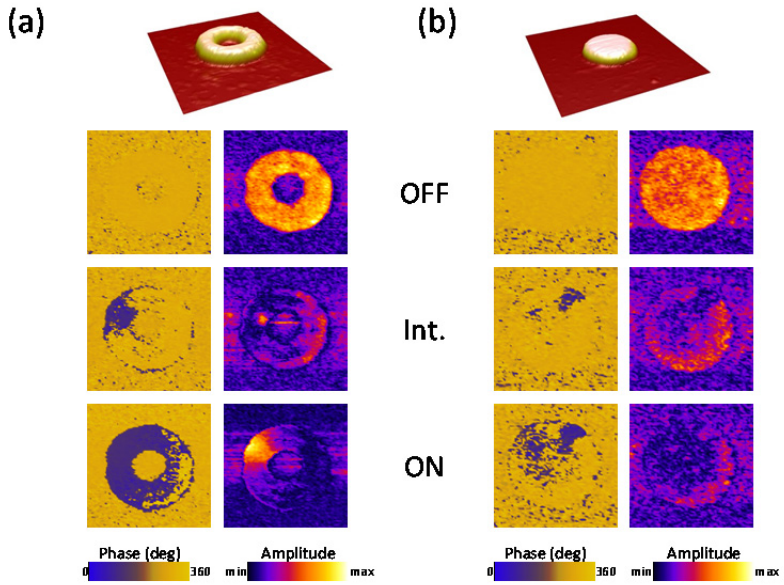

FIG. 5. Topography and piezoresponse force microscopy images (out-of-plane phase and amplitude) in the OFF, intermediate (Int.), and ON states of junctions (top to bottom) with similar areas but different shapes: (a) donut-shaped junction (500-nm and 170-nm outer and inner diameters, respectively), (b) standard circular junction (400-nm diameter). A clear difference in the switched domain configurations between the ON states of both junctions emphasizes the critical role of the border-to-area ratio that improves the switching efficiency.

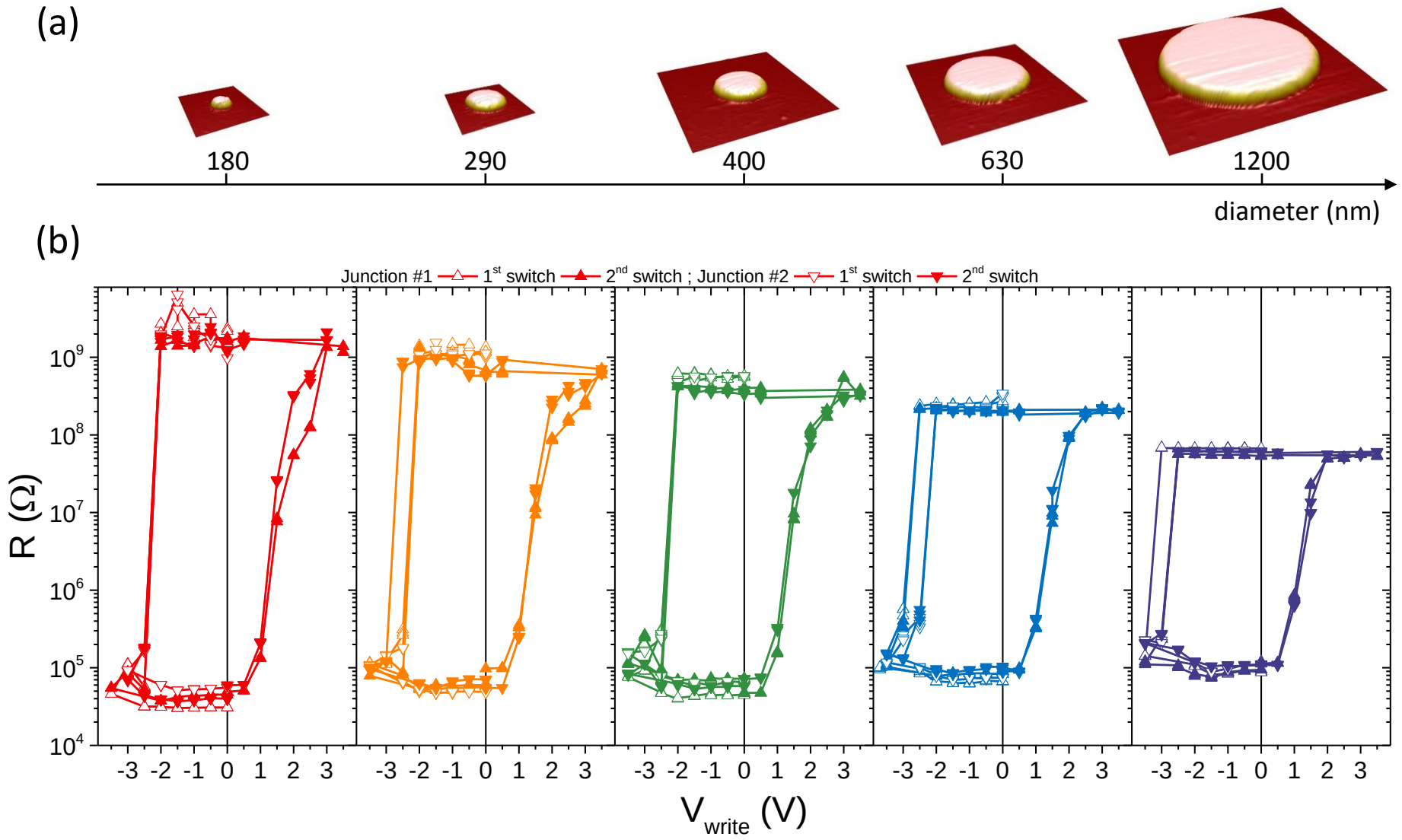
(a)
180
290
400
630
1200
diameter (nm)
(b)
Junction #1 1st switch 2nd switch ; Junction #2 1st switch 2nd switch
R (Ω)
10^9
10^8
10^7
10^6
10^5
10^4
-3 -2 -1 0 1 2 3
V write (V)

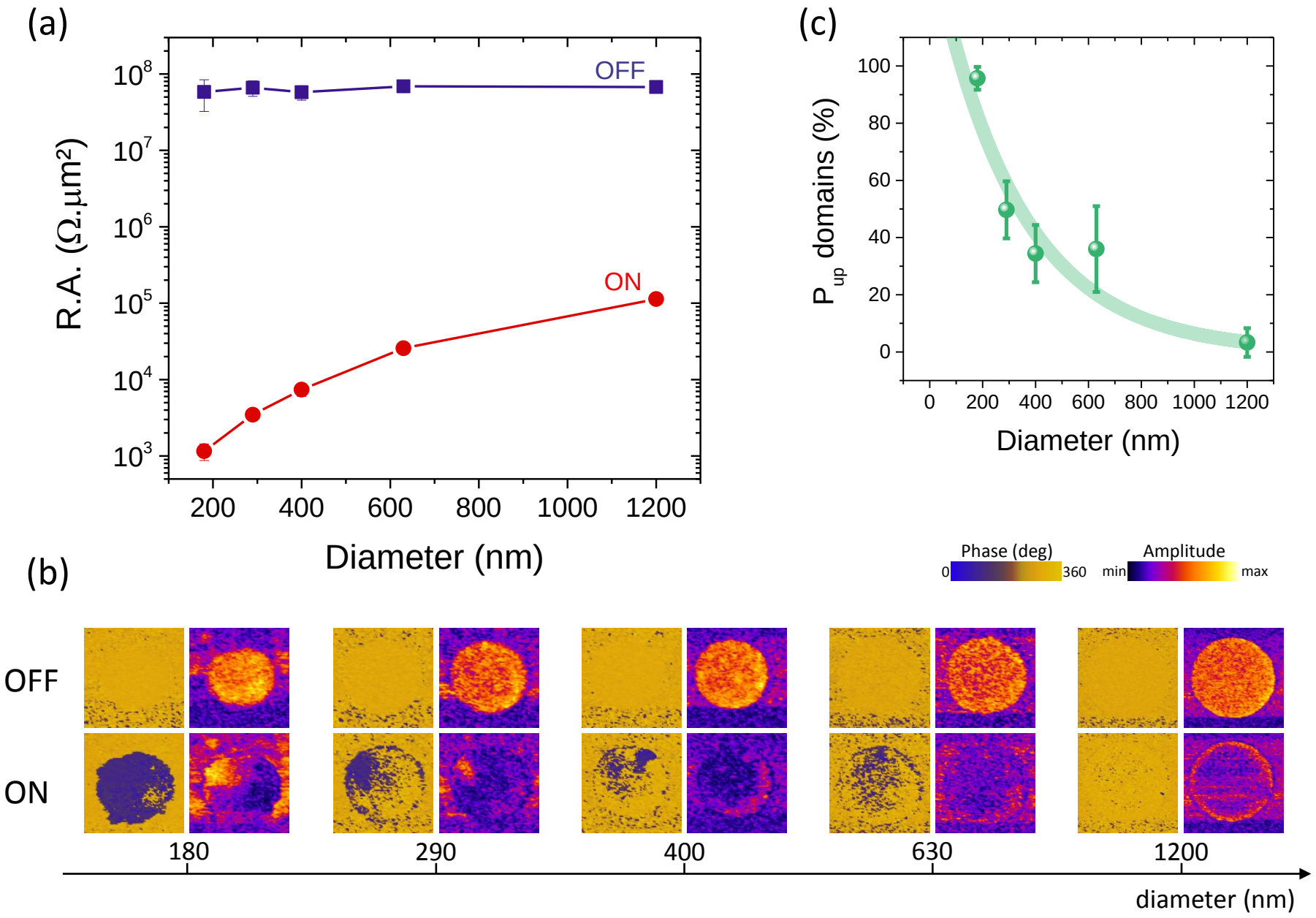
(a)
R.A. (Ω.µm²)
OFF
ON
Diameter (nm)
(c)
P up domains (%)
Diameter (nm)
(b)
Phase (deg)
0
360
Amplitude
min
max
OFF
ON
180
290
400
630
1200
diameter (nm)

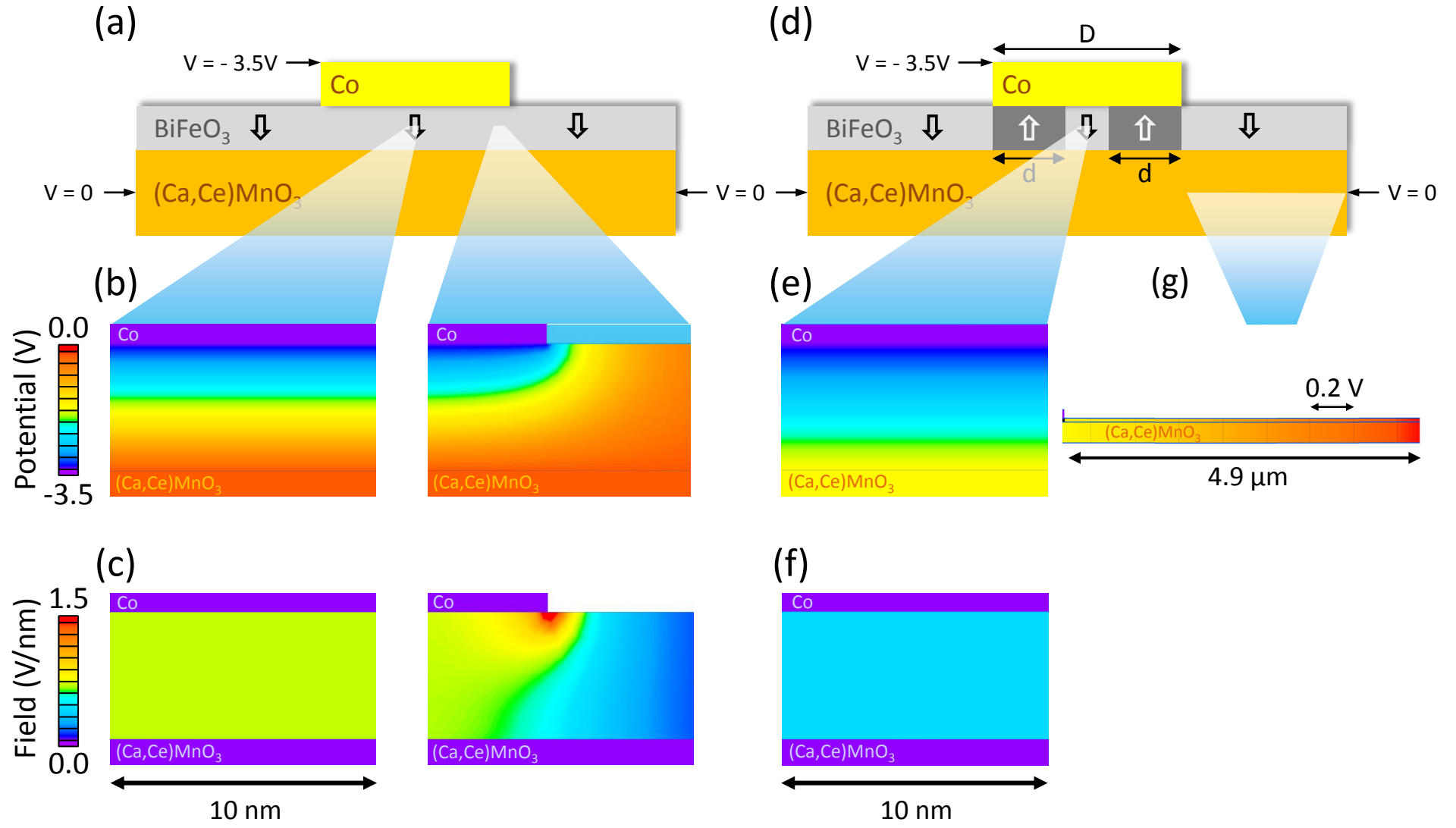
(a)
V = - 3.5V
Co
BiFeO3
(Ca,Ce)MnO3
V = 0
V = 0
(b)
Potential (V)
0.0
-3.5
Co
(Ca,Ce)MnO3
(c)
Field (V/nm)
1.5
0.0
10 nm
(d)
D
d
(e)
(f)
(g)
0.2 V
4.9 µm

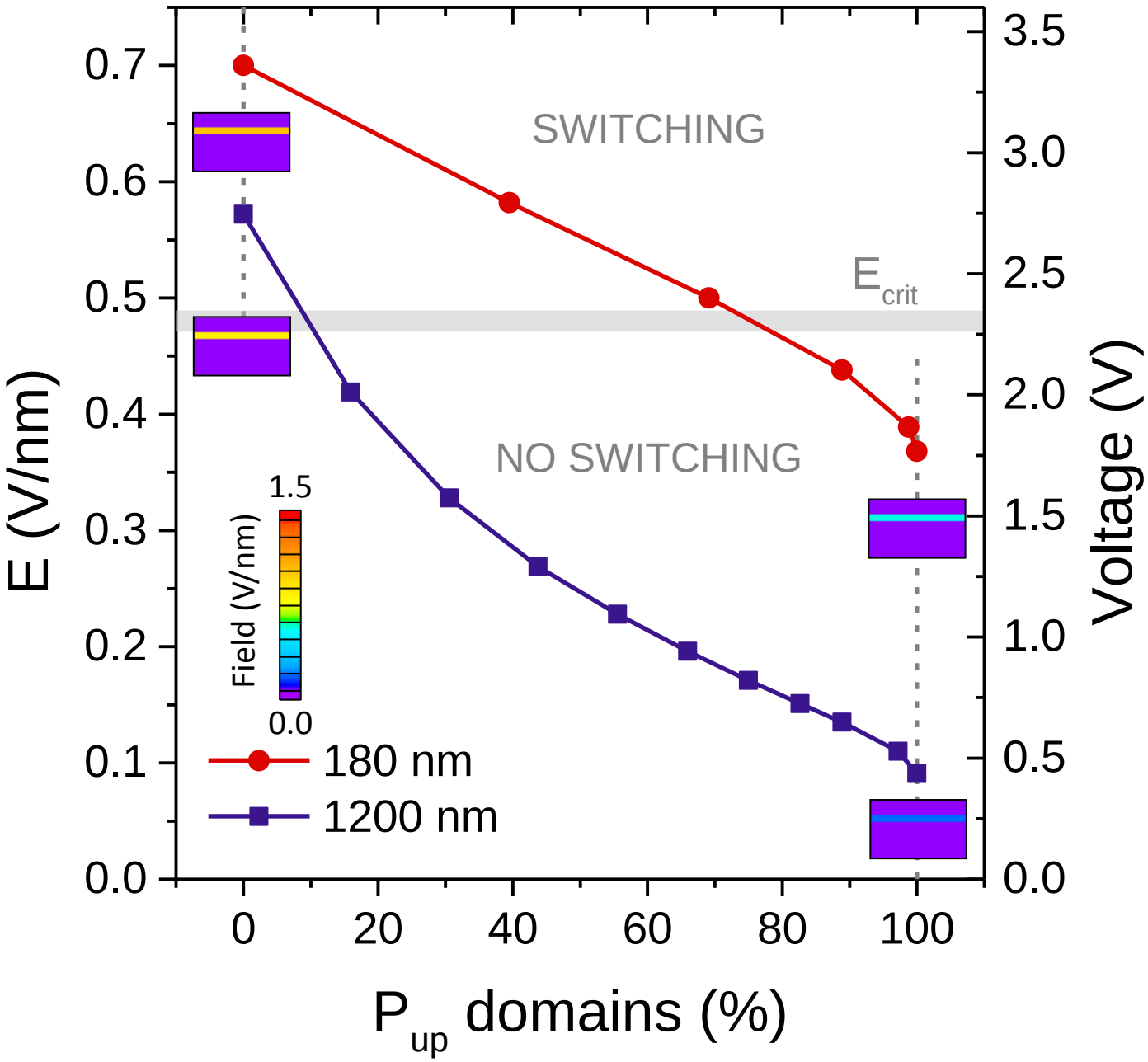
SWITCHING
NO SWITCHING
E_crit
Field (V/nm)
1.5
0.0
180 nm
1200 nm
E (V/nm)
Voltage (V)
P_up domains (%)
0.0
0.1
0.2
0.3
0.4
0.5
0.6
0.7
0.5
1.0
1.5
2.0
2.5
3.0
3.5
0
20
40
60
80
100

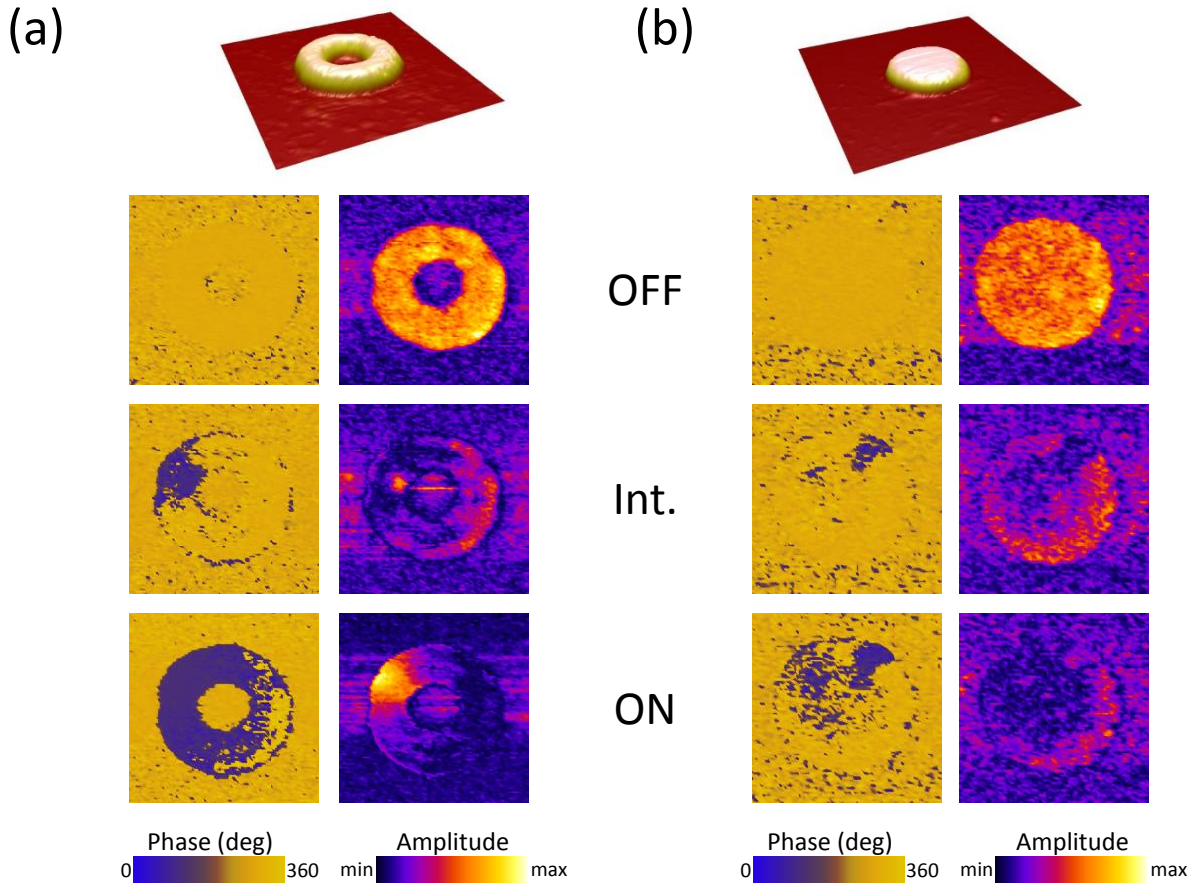
(a)
(b)
OFF
Int.
ON
Phase (deg)
0
360
Amplitude
min
max
Phase (deg)
0
360
Amplitude
min
max